Diameter-Engineered SnO_2 Nanowires over Contact-Printed Gold Nanodots Using Size-Controlled Carbon Nanopost Array Stamps

Sang Ho Lee,[†] Gunho Jo,[†] Woojin Park, Seungkyo Lee, Youn-Su Kim, Beong Ki Cho, Takhee Lee,* and Won Bae Kim*

Department of Materials Science and Engineering, Program for Integrated Molecular System (PIMS), Gwangju Institute of Science and Technology (GIST), Gwangju 500-712, Republic of Korea. [†]These authors equally contributed to this work.

ABSTRACT A novel and effective methodology to control the diameters of semiconductor nanowires is reported through a versatile contact-printing method for obtaining size-controlled nanocatalysts by size-tunable carbon-based nanometer stamps. Vertically aligned carbon nanopost arrays, derived from nanoporous alumina templates, are used as the nanoscale stamps for printing of catalyst nanoparticles. The diameter of the carbon nanopost can be engineered by adjusting the pore dimension of the templates. Over the contact-printed Au nanodots in a uniform size distribution, semiconductor SnO_2 nanowires are grown *via* a vapor−liquid−solid growth mechanism. Consequently, a direct dimension correspondence is achieved between the carbon nanopost stamp, the printed Au catalyst, and the finally obtained SnO_2 nanowires. A model example of the diameter-dependent electrical properties of the semiconductor nanowires is successfully demonstrated in this work by applying three diameter-controlled SnO_2 nanowires to nanowire field effect transistors.

KEYWORDS: carbon nanopost stamps · contact-printing of catalysts · liquid ink · diameter control · SnO_2 nanowires · alumina templates · field effect transistors

One-dimensional (1D) nanostructures are of considerable interest as an advanced building block for the next generation nanodevices because of their promising and fascinating properties.[1,2] In particular, semiconductor nanowires (NWs) have attracted significant attention for diverse applications in electronic,[3−5] photonic,[6−8] sensing,[9−12] and energy conversion[13−15] devices. For successful implementation in these applications, however, the ability to tightly define the diameter of the semiconductor NWs is becoming indispensable because their fundamental properties are strongly dependent on the radial dimension.[16−19] Therefore, there have been increasing demands for the development of new efficient methods that precisely control the NW geometries for more practical applications.

A vapor−liquid−solid (VLS) growth process has been considered as an effective synthetic technique for semiconductor NWs with a good level of geometries. Based on the VLS growth mechanism,[20] unidirectional growth is promoted by metallic catalysts in a controlled condition,[21] where the catalytic metal forms its liquid alloy that is combined with vaporized growth sources. The diameter of NWs is likely determined by the size of the alloy droplet, which is in turn governed by the original catalyst dimension. Consequently, to define the radial dimension of the desired NWs, the size of the catalysts must be predetermined and controlled. Several approaches such as narrowly size-controlled metal colloids,[22] thickness-controlled metal thin film,[23] and geometry-regulated electron-beam (E-beam) lithography[24] have been proposed to regulate the diameters of NWs in the VLS mechanism; however, these methods hold several drawbacks such as nanoparticle agglomeration,[25] wide catalyst size deviation,[26] and high fabrication cost,[27] respectively.

A contact-printing technique that uses a topographically patterned stamp, which is a representative form of soft lithography,[28] has been extensively employed in nanofabrication due to its ability to simply transfer various classes of materials from metallic compounds[29] to biological molecules[30] onto various substrates[31] in a large area at one time. The contact-printing process with a well-defined nanometer-scale stamp could be an effective tool for the designed catalyst formation in the VSL process, enabling prevention of the problems involved in the conventional methods. For instance, (1) proper placement of nanoparticle catalysts *via* printing a stamp with a

*Address correspondence to tlee@gist.ac.kr, wbkim@gist.ac.kr.

Received for review September 5, 2009 and accepted March 12, 2010.

Published online March 17, 2010.
10.1021/nn100197u

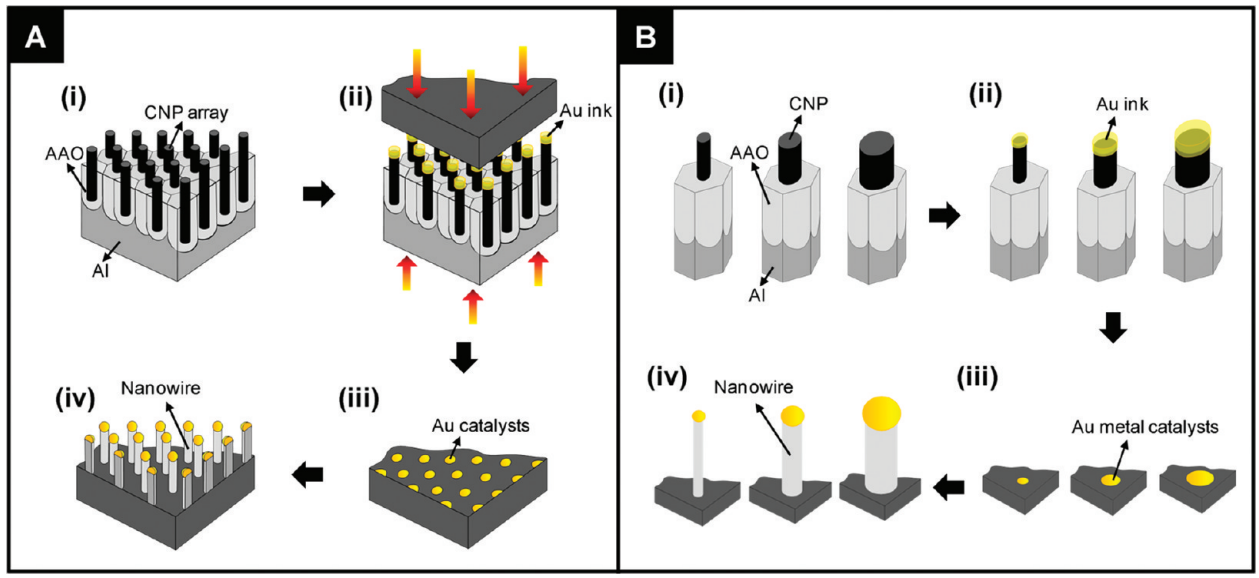

Figure 1. The schematic diagrams depict (A) the entire procedure, which includes (i) the fabrication of the CNP stamps, (ii) the contact-printing of the Au ink, (iii) the preparation of the Au metallic catalysts, and (iv) the growth of the semiconductor NWs over the contact-printed Au catalysts *via* the VLS process; and (B) the conceptual model of the size-controlled fabrication of semiconductor NWs *via* the contact-printing process using the CNP stamps with different tip diameters: (i) different-sized CNP tips, (ii) Au ink that was loaded onto the CNP tips, (iii) contact-printed Au catalysts from the CNP tips, and (iv) NWs grown over the size-controlled Au catalysts. The variation of the CNP diameter, which was used as the stamps for contact-printing of the Au catalysts, directly controls the diameter of the NWs that are grown over the printed Au particles.

predetermined geometry could prevent aggregation of the catalytic particles on substrates, (2) well-controlled stamp could produce the printed catalysts with a very narrow size distribution, and (3) the contact-printing technique could provide an intrinsic low-cost nature. However, despite these attractive features, an attempt to control the diameters of semiconductor nanowires through this printing method with nanoscale stamp has rarely been tried.

In this research, we report a novel approach that defines the diameter of the semiconductor NWs *via* a versatile contact-printing process with readily size-tunable nanoscale stamps. A vertically aligned carbon nanopost (CNP) array, fabricated from the pores of anodic aluminum oxide (AAO) templates, is used as the nanoscale stamps (denoted as CNP stamp hereafter) for printing of nanodot catalysts. The geometry of the CNP stamps is defined in the elaborated AAO templates, whose dimension is in turn controlled by modifying the pore size of the AAO matrixes. Using this approach, the diameter-controlled SnO_2 NWs are synthesized over the size-defined Au nanocatalysts in a vapor−liquid−solid (VLS) growth mechanism through a chemical vapor deposition (CVD) process. To this end, the diameter-dependent electrical characteristics of the semiconductor SnO_2 NWs are successfully and explicitly demonstrated in the nanowire field effect transistor (NW-FET), which suggests that our nanostamping methodology is an attractive strategy toward more practical applications for the fabrication of nanomaterials and nanodevices with desired functionalities.

RESULTS AND DISCUSSION

The entire procedure and conceptual cartoons for the diameter-controlled growth of semiconductor NWs *via* the contact-printing method with our CNP stamps are schematically illustrated in Figure 1. The synthesis was accomplished in four steps (Figure 1A). The first step is the fabrication of CNP stamps that have controlled CNP diameters (Figure 1A(i)), which can be achieved by regulating the pore size of the AAO matrixes (see the detail descriptions about each process in Experimental Section and Supporting Information). Next, Au precursor-containing liquid ink is coated onto the CNP array tips *via* a spin-casting process, and then it is subsequently contact-printed to the Si/SiO_2 substrate (Figure 1A(ii)). To form the metallic Au catalysts, an annealing process is conducted (Figure 1A(iii)). Finally, SnO_2 NWs are grown *via* the VLS-CVD growth process over the printed Au catalysts (Figure 1A(iv)). The diameter of the SnO_2 NWs strongly depends on the tip size of the CNP array, which makes the contact-printing process eligible for diameter-controlled growth of semiconductor NWs in the VLS system. As schematically described in Figure 1B, the tip diameter of the CNP arrays can be easily adjusted by varying the pore size of the AAO templates (Figure 1B(i)). According to the CNP diameter, the loading amount and the effective contact area of Au ink can be manipulated (Figure 1B(ii)). The size of the Au catalysts printed on the substrate is dependent on the size of ink loaded on the CNP tip (Figure 1B(iii)), and the diameter of the grown NWs is constrained to the size of the printed Au catalysts (Figure 1B(iv)). Consequently, a direct size correspondence

from the CNP stamps to the grown NWs can be achieved. This schematic diagram describes our conceptual procedures for the diameter-controlled growth of semiconductor NWs over the nanocatalysts that are contact-printed on substrates by our CNP array stamps, in which the scale and geometric dimensions are arbitrary.

The contact-printing techniques or template-based methods have been employed for fabrications of 1D nanostructures that were grown on the patterned nanoparticle catalysts,[32−35] in which patterned growths of 1D nanostructures can be achieved. Typically, contact-printing process has many attractive merits including a simple and low-cost printing process, great versatility, and high throughput. However, this method suffers from some drawbacks that include expensive and sophisticated procedures to fabricate a nanoresolution stamp and to control its size.[36,37] In our nanostamping system with the CNP array stamps, these obstacles may be overcome. Figure 2 panels a−c show representative scanning electron microscopy (SEM) images of the CNP stamps that were used here. All of the preparation procedures for the CNP stamps were composed of a simple self-assembly process without conventional nanopatterning methods, such as photolithography or E-beam lithography. Precisely controlled CNP arrays were fabricated by depositing pyrolytic carbon onto the inside surfaces of straight pore channels that were self-assembled in the AAO matrixes, and followed by simple mechanical and chemical treatments (see the Experimental Section and Figure S1 of the Supporting Information). Three representative stamps (Figure 2a−c) exhibit monodispersed CNP diameters of 33 ± 3, 46 ± 3, and 78 ± 4 nm, respectively. Modification of the stamp size can be readily achieved by adjusting the pore dimension of the AAO templates, as confirmed from Figure 2d, which shows a direct correlation between the AAO pore size and the CNP tip diameter. As the pore size of the AAO template increases from 30 to 80 nm, the tip diameter of the produced CNP increases in a consistent manner. SEM images of the tilt views (the insets of Figure 2a−c) show the geometrical characteristics of the CNP arrays with a flat top surface and a uniform height of *ca.* 100 nm protruding from the AAO template.[38] The vertically aligned CNP arrays with a homogeneous height, which are combined with their own flexibility that originated from carbon,[39,40] could bear the applied force in a direction that is perpendicular to the tips during the contact-printing process. As a consequence of the reliable nanoscale size, simple size-controllability and uniform height, the CNP stamps could be an elegant platform for a nanostamping system that prints size-controlled catalysts for diameter-controlled growth of various semiconductor NWs.

Figure 3 panels a, b, and c show representative SEM images of the contact-printed Au catalysts on the Si/SiO_2 substrate by using the CNP stamps that have the

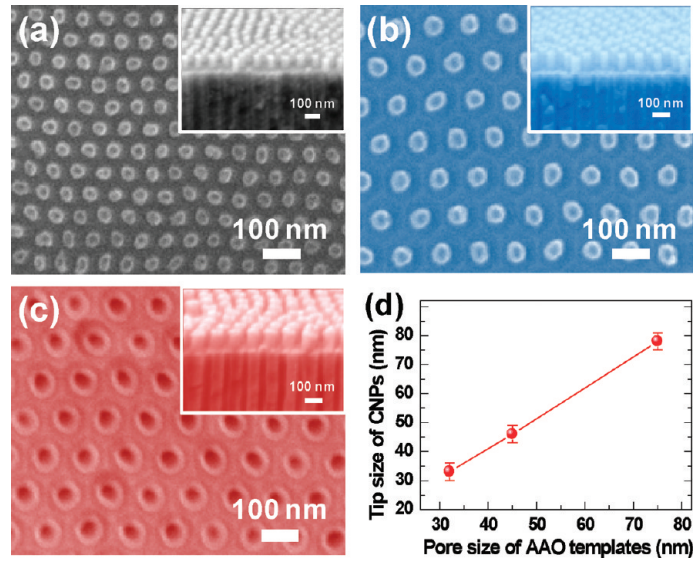

Figure 2. SEM images of the CNP stamps that have different tip diameters of (a) 33, (b) 46, and (c) 78 nm. Each inset of panels a−c is an oblique view, which indicates that the CNP arrays have a uniform height of *ca.* 100 nm. (d) The direct correspondence between the average tip diameter of the CNP arrays and the pore size of the AAO templates. The error bars represent the deviation of the CNP diameter that was estimated from 100 different CNPs.

average tip diameters of 33, 46, and 78 nm, respectively. The histograms for the size distribution of Au nanoparticles in the insets indicate narrow size-

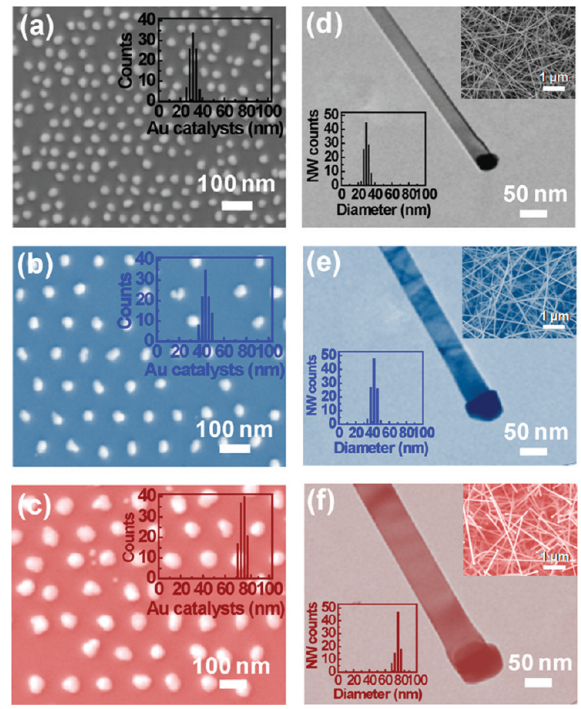

Figure 3. SEM images of the contact-printed Au catalysts that display the average size of (a) 30, (b) 42, and (c) 71 nm, respectively (Insets show the histograms of the printed Au nanoparticles). TEM micrographs of grown SnO_2 NWs of (d) 32, (e) 43, (f) 77 nm in diameter, which were initiated over the printed Au catalysts. The SEM images of the upper insets display the SnO_2 NWs grown on the Au-catalyst-printed substrate. The histograms of the lower insets indicate a narrow diameter deviation of the grown SnO_2 NWs.

deviations with slight size decreases (by *ca.* 10%) from the tip sizes of the CNP stamps; the printed Au nanoparticles display the mean sizes of 30, 42, and 71 nm, respectively. This size contraction of the printed catalysts should be ascribed to the evaporation of ethanol solvent in the as-printed Au ink and is also accompanied by the phase transformation of the Au phase from the ink to the metallic phase during the annealing process (see Figure S5 of the Supporting Information for this phase transformation process). Considering the accuracy of the contact-printed Au nanocatalysts in terms of geometric pattern and transfer yield, it seems that a perfect pattern replication was not achieved at the present condition because some defect sites in the printed Au nanoparticles appear in the SEM images of Figure 3a−c. We speculate that the involvement of such defects in the printed Au nanoparticles may be attributable to the possibly insufficient loading of the Au ink solution onto the individual tips of the CNP arrays when the liquid phase ink solution is used for the contact-printing process. Despite the presence of defects, the pattern accuracy and transfer yield were quantitatively analyzed. The transfer yield is estimated to approximately 80% or higher for all the samples in this work, which is a fraction of the number of the printed Au nanoparticles to the number of the CNP tips in the same unit area. Note the SEM images of Figure S4 and the description for the transfer yield in the Supporting Information. However, if the ink is properly made and optimized further, a better replication close to the perfect pattern from the mother CNP stamps would be possible. Indeed, the hexagonally patterned Au nanodot arrays with the least defects were able to be fabricated *via* the same contact-printing method through direct loading of the metallic Au on the CNP arrays by an E-beam evaporation process (which is under development and its detailed procedure is described in the reference as a note.)[41] Although some defects are generated when the liquid phase ink is used in this work, still a number of advantages can be expected from the use of the liquid phase ink in the face of simplicity of the process, reusability of the stamps, and wide availability of the catalyst ink materials. It is demonstrated that the morphology of the CNP stamp can be maintained even after repeated stamping processes (see Figure S3 of the Supporting Information) along with the easy cleaning with solvent for the ink remnant. Moreover, numerous catalyst materials can be applied in this liquid ink system as far as the catalyst precursor salt is dissolved in the solvent, implying that this process can be extended to other fascinated 1D nanostructure growths such as GaN NWs[42] and carbon nanotubes.[43]

Figure 3 panels d−f show typical transmission electron microscopy (TEM) images of the SnO_2 NWs that were grown over the contact-printed Au catalysts *via* the VLS-CVD process. The TEM samples were prepared

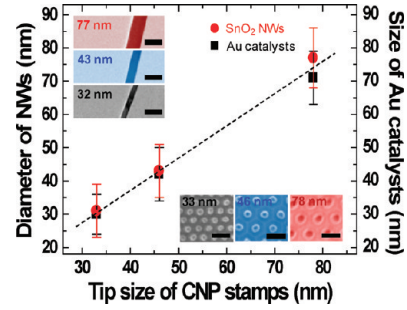

Figure 4. The size correspondence between the Au catalysts and the grown SnO_2 NWs with respect to the CNP tip diameters of the stamps that were used for contact-printing. Here, the average diameter and the error value of the samples were determined statistically from the SEM and TEM images. The lower insets show the SEM images of three different CNP stamps that were used in this work. The upper inset shows TEM images of the as-grown SnO_2 NWs that have controlled diameters. All of the scale bars indicate 100 nm.

by sonicating the as-grown NWs (the SEM images in upper insets) into a suspension in isopropyl alcohol and then followed by depositing onto a TEM copper grid. The SnO_2 NWs represent a smooth and straight-line morphology together with the alloy droplets shown at the end part of each NW. Such catalyst-mediated nanowire growth may support that our diameter-tunable process is associated with the VLS mechanism. The diameter of the obtained SnO_2 NWs appeared to be about 32, 43, and 77 nm, respectively, which would be a little bit increased but still in a tight correspondence on the printed catalyst sizes.[20] Both the high-resolution TEM images and their selective area electron diffraction (SAED) patterns (see Figure S6 of the Supporting Information) indicate that the obtained SnO_2 NWs are of a single-crystalline phase in a tetragonal rutile structure. The diameter distribution of the SnO_2 NWs was statistically analyzed from the detailed SEM and TEM inspection. From the histograms of the NW's diameter as included in the lower insets of Figure 3 panels d−f, we were able to confirm that the SnO_2 NWs synthesized *via* our method are nicely controllable in a uniform diameter.

Figure 4 summarizes a direct and excellent linear correlation of size dimensions between the mother CNP stamps, the printed Au catalysts from the stamps, and the finally grown SnO_2 NW over the catalysts, which would represent one of the strengths of our method. As a result of contact-printing with the CNP stamps having 33, 46, and 78 nm diameter (lower inset SEM images), the Au catalysts were printed with average diameters of *ca.* 30, 42, and 71 nm, respectively, and in the event, the SnO_2 NWs were grown with mean diameters of *ca.* 32, 43, and 77 nm (upper inset TEM images). This result clearly demonstrates that our contact-printing method by using the size-tunable CNP stamp is significantly promising for the fabrication of semiconductor NWs in the VLS system, especially in regard of high

throughput production along with engineering of designed radial dimension.

This diameter-tuning of semiconductor NWs has motivated us to a fundamental study on the intrinsic electrical properties with the systematically changed radial dimensions. A representative example of the diameter-dependent properties was demonstrated from nanowire field effect transistors (NW-FETs) fabricated in a back-gated configuration using the three diameter-controlled SnO_2 NWs.[44−46] Figure 5a illustrates the configuration of SnO_2 NW-FETs used here. Figure 5b shows a series of SEM images for each single SnO_2 NW that connects across the source and drain electrodes. The respective diameter (d_{NW}) of SnO_2 NW was 32, 43, and 77 nm, as confirmed previously. From the transfer characteristics ($I_{DS}-V_{GS}$, the source−drain current *versus* gate voltage) in Figure 5c, the SnO_2 NW-FETs exhibit the typical n-type semiconductor characteristics. As the NW diameter in the FET devices is increased, the threshold voltage (V_T) shifts to the negative gate bias direction and the source−drain current appears to increase for a given gate bias, which is in line with the results reported by other research groups.[44] The threshold voltage of the three different SnO_2 NW FETs shown in Figure 5c (d_{NW} = 32, 43, and 77 nm) was found to be −4.34, −5.97, and −7.87 V, respectively. The increased effective channel area of the larger diameter NWs is responsible for such consistent V_T shifts. It is known that the depletion region can build up by the interface states and trapped charges, leading to affecting the electronic transport characteristics of the NWs.[47,48] A schematic illustration and band diagram for our devices (see Figure S9 of the Supporting Information) explain the discrepancy between the geometrical diameter (d_{NW}) and the effective diameter (d_{eff}) that is considered with the depletion width (w). The surface band bending at the interfaces between the NW and its surroundings is associated with the depletion width formation. The effective diameter (d_{eff}) of the conduction layer in the NW channel can be expressed as $d_{eff} = d_{NW} - 2w$. Therefore, larger diameter NWs can have a larger d_{eff}/d_{NW} ratio than smaller diameter NWs since the wider NW can generate a more significant conductive channel fraction as compared to the smaller diameter NWs, implying that it becomes easier to create an accumulation channel for a given gate bias. As a consequence, in the NW FETs with a larger diameter, the conductance increases and the threshold voltages shift in the negative gate bias direction.

From the transfer characteristics (Figure 5c), the field-effect mobility values ($\mu_{FE,e} = L^2/C_{NW}V_{DS}(\partial I_{DS}/\partial V_{GS})$)[49] of the SnO_2 NW-FETs were estimated to be 94, 125, and 179 $cm^2/(V\ s)$ for the three NWs with different diameters, d_{NW} of 32, 43, and 77 nm, respectively (see Table S1 of the Supporting Information). The observed dependence of the SnO_2 NW diameter on their mobility reveals that the larger diameter NWs possess significantly higher mobility than the smaller ones, which may be explained by the enhanced surface scattering (i.e., surface roughness and defect scattering).[26,27] The effect of side-wall scattering in the overall mobility will be greater in smaller diameter NWs than in larger ones.[50−52] In addition, the field-effect mobility is generally smaller in narrower NWs because of the lower effective gate coupling factor. This is ascribed to that the interface states attract negative charge to the n-type NW surface, which has a stronger influence on the miniaturized NWs with a high surface area to volume ratio.[50,53] The inset of Figure 5c shows the statistical distribution of the threshold voltage and the field-effect mobility, as a function of the average NW diameters of 32 nm (measured from 17 NW-FETs), 43 nm (from 12 NW-FETs), and 77 nm (from 5 NW-FETs), respectively. Therefore, statistically it can be concluded that the change in the diameter of the NWs can have a significant influence on the electronic transport properties due to the alteration of the surface area to volume ratio. Therefore, the diameter-tuning of semiconductor

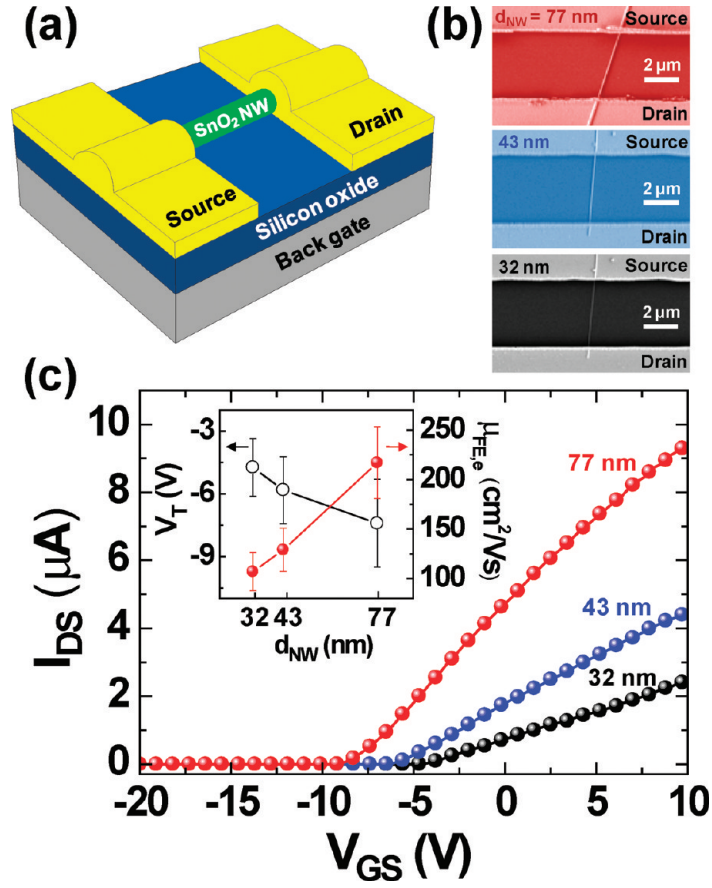

Figure 5. (a) A schematic diagram of a SnO_2 NW-FET. (b) SEM images of diameter-controlled SnO_2 NW-FETs with d_{NW} of 77, 43, and 32 nm, respectively. The channel lengths of the three different SnO_2 NW-FETs were *ca.* 4 μm. (c) The transfer characteristics ($I_{DS}-V_{GS}$) for the SnO_2 NW-FETs at a fixed drain bias of 1 V for the d_{NW} of 77, 43, and 32 nm. The inset shows the statistical distribution of the threshold voltage (V_T, open black symbols) and the field effect mobility ($\mu_{FE,e}$, filled red symbols) for 17 FET devices that were made with a d_{NW} of 32 nm, 12 FET devices that were made with a d_{NW} of 43 nm, and 5 FET that were devices made with a d_{NW} of 77 nm, respectively.

nanowires *via* the contact-printing process using the size-controllable CNP stamps can play an effective role in the fabrication of nanostructures and the design of nanoscale devices, as demonstrated with the diameter-controlled SnO_2 NWs in this work.

CONCLUSION

In conclusion, we reported a simple and effective method for fabrication of semiconductor nanowires having a designed diameter *via* a contact-printing method that uses size-tunable carbon-based nanopost array stamps. This versatile contact-printing technique enables control of the size of printed nanoparticle catalysts, thereby the diameter of semiconductor nanowires can be manipulated depending on the catalyst size in the vapor−liquid−solid growth process. Diameter-dependent electrical properties of the controlled SnO_2 nanowires were explicitly embodied by the application to nanowire field effect transistors. The ability to control a well-defined radial dimension of the semiconductor nanowires could facilitate implementation of one-dimensional nanoscale building-blocks in various nanodevices. Although we demonstrated only for the SnO_2 nanowires at this stage, this method could be equally applied to other one-dimensional nanostructure growths of various materials, which is under investigation along with modifications of catalyst transfer steps.

EXPERIMENTAL SECTION

Fabrication of the CNP Stamps. Three kinds of CNP stamps that have a controlled-tip diameter were prepared by replicating the AAO pores of three different sizes. First, the AAO templates were produced through a two-step anodization process under controlled voltages. For the AAO template with small-sized pores of *ca.* 33 nm, prepolished Al foils (99.999%) were anodized in a 0.3 M H_2SO_4 solution under 25 V, while the Al foils were anodized in a 0.3 M $H_2C_2O_4$ solution under 40 V for the AAO template with middle-sized pores of *ca.* 46 nm. From further pore-widening of the AAO matrix (produced in 0.3 M $H_2C_2O_4$ electrolyte) by chemical-wet etching in a mixture solution of H_3PO_4 and CrO_3, the AAO template with a large pore size of *ca.* 78 nm was obtained. Next, deposition of the carbon layer throughout the surfaces of the prepared alumina templates was conducted by a thermal chemical vapor deposition (CVD) method at 600 °C in a gas mixture of C_2H_2 and NH_3 without any catalysts. Finally, for the selective exposure of the CNP arrays out of the AAO matrix, a dry-etching *via* ion-milling was performed and subsequently followed by chemical-wet etching in an etching solution, which resulted in the CNP stamps. The pore sizes of the AAO templates and the exposure lengths of the CNP arrays can be finely controlled as reported previously.[54]

Printing of the Gold Catalysts. Before the contact-printing process, our CNP stamps and Si/SiO_2 substrates were cleaned, and then they were treated with oxygen plasma in order to enhance the surface wetting property. Although the stamps can be reused for multiple stamping, in all of the experiments, fresh stamps were used to avoid interference from the transference of leftover ink to the next print process. The liquid phase Au ink was prepared by mixing chloroauric acid ($HAuCl_4 \cdot 3H_2O$, 0.4 g) and poly(vinylpyrrolidone) (PVP, 0.02 g) in ethanol solution (8 mL), in which the PVP additive may function to decrease rapid evaporation of the ethanol solvent and to increase the viscosity of the ink phase for an efficient loading and transferring process. The Au ink was dispersed onto the tips of the CNP stamp *via* a spin-coating process at 4000−6000 rpm for 30 s; subsequently, the ink-loaded CNP stamp was transferred and contacted onto the pretreated Si/SiO_2 substrate in a conformal way. In the contact-printing process, the CNP stamp was positioned under the substrate in order to minimize excessive ink-printing (see Figure 1A(ii)). The as-printed Au ink phases were first heat-treated in an oven at 70 °C to evaporate the solvent from the substrate, and then the samples were annealed at 500 °C in the air for 4 h to transform the Au salt phase to the metallic Au phase. These heat treatments lead to a slight size discrepancy between the CNP stamps and the printed Au nanoparticles.

Growth of the SnO_2 NWs. The SnO_2 NWs were synthesized over the contact-printed Au catalysts through a carbothermal reduction that was followed by the CVD method *via* the VLS growth mechanism. An alumina boat that contains a 2:1 powder mixture (by weight) of SnO_2 (99.99% purity) and graphite (99.995% purity) was loaded at the center of a horizontal quartz tube. The Au-catalyst-printed substrate was placed downstream (3−5 cm) from the center of the quartz tube. After the system was evacuated under 200 sccm of Ar gas flow (99.999% purity), the reactor was heated up to 900 °C at a ramping rate of 10 °C min^{-1} and kept at that temperature with the Ar carrier gas for 20−60 min. After the furnace was cooled to room temperature, light gray products were observed on the surface of the substrate.

Fabrication of the NW-FET Devices. To fabricate the SnO_2 NW-FET devices, the grown SnO_2 NWs were transferred from the growth substrate by dropping and drying the NW suspension to a Si wafer with a 100-nm thick thermally grown oxide layer. The NW suspension was made by briefly sonicating the growth substrate of the SnO_2 NWs in isopropyl alcohol for 30 s. The Si wafers that were used in this study were highly doped p-type substrates, which can serve as a back gate electrode. Metal electrodes that consist of Ti (30 nm)/Au (40 nm) were deposited by an E-beam evaporator to provide the ohmic contact with the SnO_2 NW. The electrodes were defined as either the source or drain by a photolithography and lift-off process. The distance between the source and drain electrode was approximately 4 μm. The current−voltage transfer characteristics of the transistors were measured with a semiconductor parameter analyzer (Agilent B1500A) in an ambient atmosphere.

Acknowledgment. This work was supported by the National Research Foundation of Korea (NRF) grant funded by the Korea government (MEST) (No. R15-2008-006-03002-0 and No. 20090058918). Also, we are grateful to the Program for Integrated Molecular Systems (PIMS/GIST) for the financial support.

Supporting Information Available: Detailed fabrication procedure for the CNP stamps, SEM images of the AAO templates with three different-sized pores, reusability test of the CNP stamps, transfer yield analysis of the printed Au nanoparticles, morphology comparison of the printed Au phases before and after annealing treatment, TEM and XRD analysis of the grown SnO_2 NWs, summary of the SnO_2 NW-FET device parameters, transconductance (g_m) and field-effect mobility ($\mu_{FE,e}$) data, the $I_{DS}-V_{GS}$ curve, and effective diameter (d_{eff}). This material is available free of charge *via* the Internet at http://pubs.acs.org.

REFERENCES AND NOTES

1. Lieber, C. M.; Wang, Z. L. Functional Nanowires. *MRS Bull.* **2007**, *32*, 99–104.
2. Xia, Y.; Yang, P.; Sun, Y.; Wu, Y.; Mayers, B.; Gates, B.; Yin, Y.; Kim, F.; Yan, H. One-Dimensional Nanostructures: Synthesis, Characterization, and Applications. *Adv. Mater.* **2003**, *15*, 353–389.
3. Ju, S.; Li, J.; Pimparkar, N.; Alam, M. A.; Chang, R. P. H.; Janes, D. B. N-Type Field-Effect Transistors Using Multiple Mg-Doped ZnO Nanorods. *IEEE Trans.Nanotechnol.* **2007**, *6*, 390–395.

4. Xiang, J.; Lu, W.; Hu, Y.; Wu, Y.; Yan, H.; Lieber, C. M. Ge/Si Nanowire Heterostructures as High-Performance Field-Effect Transistors. *Nature* **2006**, *441*, 489–493.
5. Dayeh, S. A.; Aplin, D. P. R.; Zhou, X.; Yu, P. K. L.; Yu, E. T.; Wang, D. High Electron Mobility InAs Nanowire Field-Effect Transistors. *Small* **2007**, *3*, 326–332.
6. Bao, J.; Zimmler, M. A.; Capasso, F.; Wang, X.; Ren, Z. F. Broadband ZnO Single-Nanowire Light-Emitting Diode. *Nano Lett.* **2006**, *6*, 1719–1722.
7. Gubbala, S.; Chakrapani, V.; Kumar, V.; Sunkara, M. K. Band-Edge Engineered Hybrid Structures for Dye-Sensitized Solar Cells Based on SnO_2 Nanowires. *Adv. Funct. Mater.* **2008**, *18*, 2411–2418.
8. Ju, S.; Li, J.; Liu, J.; Chen, P. -C.; Ha, Y. -g.; Ishikawa, F.; Chang, H.; Zhou, C.; Facchetti, A.; Janes, D. B.; *et al*. Transparent Active Matrix Organic Light-Emitting Diode Displays Driven by Nanowires Transistor Circuitry. *Nano Lett.* **2008**, *8*, 997–1004.
9. Cui, Y.; Wei, Q.; Park, H.; Lieber, C. M. Nanowire Nanosensors for Highly Sensitive and Selective Detection of Biological and Chemical Species. *Science* **2001**, *293*, 1289–1292.
10. Soci, C.; Zhang, A.; Xiang, B.; Dayeh, S. A.; Aplin, D. P. R.; Park, J.; Bao, X. Y.; Lo, Y. H.; Wang, D. ZnO Nanowire UV Photodetectors with High Internal Gain. *Nano Lett.* **2007**, *7*, 1003–1009.
11. Wang, B.; Zhu, L. F.; Yang, Y. H.; Xu, N. S.; Yang, G. W. Fabrication of a SnO_2 Nanowire Gas Sensor and Sensor Performance for Hydrogen. *J. Phys. Chem. C* **2008**, *112*, 6643–6647.
12. Shen, G.; Chen, P. -C.; Ryu, K.; Zhou, C. Devices and Chemical Sensing Applications of Metal Oxide Nanowires. *J. Mater. Chem.* **2009**, *19*, 828–839.
13. Shim, H. -S.; Na, S. -I.; Nam, S. H.; Ahn, H. -J.; Kim, H. J.; Kim, D. -Y.; Kim, W. B. Efficient Photovoltaic Device Fashioned of Highly Aligned Multilayers of Electrospun TiO_2 Nanowire Array with Conjugated Polymer. *Appl. Phys. Lett.* **2008**, *92*, 183107.
14. Kim, Y. -S.; Ahn, H. -J.; Nam, S. H.; Lee, S. H.; Shim, H. -S.; Kim, W. B. Honycomb Pattern Array of Vertically Standing Core−Shell Nanorods: Its Application to Li Energy Electrodes. *Appl. Phys. Lett.* **2008**, *93*, 103104.
15. Fan, Z.; Razavi, H.; Do, J. -W.; Moriwaki, A.; Ergen, O.; Chueh, Y. -L.; Leu, P. W.; Ho, J. C.; Takahashi, T.; Reichertz, L. A.; *et al* . Three-Dimensional Nanopillar-Array Photovoltaics on Low-Cost and Flexible Substrates. *Nat. Mater.* **2009**, *8*, 648–653.
16. Léonard, F.; Talin, A. A.; Swartzentruber, B. S.; Picraux, S. T. Diameter-Dependent Electronic Transport Properties of Au-Catalyst/Ge-Nanowire Schotty Diodes. *Phys. Rev. Lett.* **2009**, *102*, 106805.
17. Liu, Z.; Zhang, D.; Han, S.; Li, C.; Tang, T.; Jin, W.; Liu, X.; Lei, B.; Zhou, C. Laser Ablation Synthesis and Electron Transport Studies of Tin Oxide Nanowires. *Adv. Mater.* **2003**, *15*, 1754–1757.
18. Mathur, S.; Barth, S.; Shen, H.; Pyun, J. -C.; Werner, U. Size-Dependent Photoconductance in SnO_2 Nanowires. *Small* **2005**, *1*, 713–717.
19. Nam, C. -Y.; Jaroenapibal, P.; Tham, D.; Luzzi, D. E.; Evoy, S.; Fischer, J. E. Diameter-Dependent Electromechanical Properties of GaN Nanowires. *Nano Lett.* **2006**, *6*, 153–158.
20. Wu, Y.; Yang, P. Direct Observation of Vapor−Liquid−Solid Nanowire Growth. *J. Am. Chem. Soc.* **2001**, *123*, 3165–3166.
21. Qu, D. M.; Yan, P. X.; Chang, J. B.; Yan, D.; Liu, J. Z.; Yue, G. H.; Zhuo, R. F.; Feng, H. T. Nanowires and Nanowire−Nanosheet Junction of SnO_2 Nanostructures. *Mater. Lett.* **2007**, *61*, 2255–2258.
22. Gudiksen, M. S.; Lieber, C. M. Diameter-Selective Synthesis of Semiconductor Nanowires. *J. Am. Chem. Soc.* **2000**, *122*, 8801–8802.
23. Huang, M. H.; Wu, Y.; Feick, H.; Tran, N.; Weber, E.; Yang, P. Catalytic Growth of Zinc Oxide Nanowires by Vapor Transport. *Adv. Mater.* **2001**, *13*, 113–116.
24. Simpkins, B. S.; Pehrsson, P. E.; Taheri, M. L.; Stroud, R. M. Diameter Control of Gallium Nitride Nanowires. *J. Appl. Phys.* **2007**, *101*, 094305.
25. Bogart, T. E.; Dey, S.; Lew, K. -K.; Mohney, S. E.; Redwing, J. M. Diameter-Controlled Synthesis of Silicon Nanowires Using Nanoporous Alumina Membraces. *Adv. Mater.* **2005**, *17*, 114–117.
26. Li, C.; Zhang, D.; Han, S.; Liu, X.; Tang, T.; Zhou, C. Diameter-Controlled Growth of Single-Crystalline In_2O_3 Nanowires and Their Electronic Properties. *Adv. Mater.* **2003**, *15*, 143–146.
27. Hochbaum, A. I.; Fan, R.; He, R.; Yang, P. Controlled Growth of Si Nanowire Arrays for Device Integration. *Nano Lett.* **2005**, *5*, 457–460.
28. Xia, Y.; Whitesides, G. M. Soft Lithography. *Angew. Chem., Int. Ed.* **1998**, *37*, 550–575.
29. Cao, T.; Xu, Q.; Winkleman, A.; Whitesides, G. M. Fabrication of Thin, Metallic Film along the Sidewalls of a Topographically in Charge Printing. *Small* **2005**, *1*, 1191–1195.
30. Biancardo, S. B. N.; Pranov, H. J.; Larsen, N. B. Protein In-Mold Patterning. *Adv. Mater.* **2008**, *20*, 1825–1829.
31. Ko, H. C.; Stoykovich, M. P.; Song, J.; Malyarchuk, V.; Choi, W. M.; Yu, C. -J.; Geddes III, J. B.; Xiao, J.; Wang, S.; Huang, Y.; *et al*. A Hemispherical Electronic Eye Camera Based on Compressible Silicon Optoelectronics. *Nature* **2008**, *454*, 748–753.
32. Golovko, V. B.; Li, H. W.; Kleinsorge, B.; Hofmann, S.; Geng, J.; Cantoro, M.; Yang, Z.; Jefferson, D. A.; Johnson, B. F. G.; Huck, W. T. S.; *et al*. Submicron Patterning of Co Colloid Catalyst for Growth of Vertically Aligned Carbon Nanotubes. *Nanotechnology* **2005**, *16*, 1636–1640.
33. Mrtensson, T.; Carlberg, P.; Borgstrm, M.; Montelius, L.; Seifert, W.; Samuelson, L. Nanowire Arrays Defined by Nanoimprint Lithography. *Nano Lett.* **2004**, *4*, 699–702.
34. Liu, X.; Bigioni, T. P.; Xu, Y.; Cassell, A. M.; Cruden, B. A. Vertically Aligned Dense Carbon Nanotube Growth with Diameter Control by Block Copolymer Micelle Catalyst Templates. *J. Phys. Chem. B* **2006**, *110*, 20102–20106.
35. Lee, D. H.; Lee, W. J.; Kim, S. O. Vertical Single-Walled Carbon Nanotube Arrays *via* Block Copolymer Lithography. *Chem. Mater.* **2009**, *21*, 1368–1374.
36. Kumar, A.; Whitesides, G. M. Features of Gold Having Micrometer to Centimeter Dimensions Can Be Formed through a Combination of Stamping with an Elastomeric Stamp and an Alkanethiol "Ink" Followed by Chemical Etching. *Appl. Phys. Lett.* **1993**, *63*, 2002–2004.
37. Kim, J.; Takama, N.; Kim, B. Reprint of "Fabrication of Nano-Structures Using Inverse-μCP Technique with a Flat PDMS Stamp. *Sens. Actuators, A* **2007**, *139*, 356–363.
38. Park, S.; Kim, Y.-S.; Kim, W. B.; Jon, S. Carbon Nanosyringe Array as a Platform for Intracellular Delivery. *Nano Lett.* **2009**, *9*, 1325–1329.
39. Poncharal, P.; Wang, Z. L.; Ugarte, D.; de Heer, W. A. Electrostatic Deflections and Electromechanical Resonances of Carbon Nanotubes. *Science* **1999**, *283*, 1513–1516.
40. Jaroenapibal, P.; Luzzi, D. E.; Evoy, S.; Arepalli, S. Transmission-Electron-Microscopic Studies of Mechanical Properties of Single-Walled Carbon Nanotubes Bundles. *Appl. Phys. Lett.* **2004**, *85*, 4328–4330.
41. The direct metal transfer mechanism is based on the difference in the adhesion strengths between stamp−metal and substrate−metal; the surface adhesion of the metal to the substrate should be much higher than to the stamp. First, the surfaces of CNP stamps were treated by a self-assembly monolayer with $CF_3(CF_2)_5(CH_2)_2SiCl_3$ (tridecafluoro-1,1,2,2-tetrahydrooctyl-trichlorosilane), which served as an anti-sticking layer that reduces the adhesion between the CNP tips and the metallic Au particles. Next, the solid phase metallic Au ink is deposited on the tips of the surface-pretreated CNP stamps, and a thin adhesion Ti layer (< 2 nm) that reinforces the cohesion between the Au metal and the substrate is consecutively loaded on the top surface of the Au metal (both were performed by an E-beam

evaporation method at a pressure of $\sim 10^{-7}$ Torr). The metal-loaded CNP stamps are contact-printed onto the precleaned Si/SiO_2 substrates in the laboratory environment.

42. Duan, X.; Lieber, C. M. Laser-Assisted Catalytic Growth of Single Crystal GaN Nanowires. *J. Am. Chem. Soc.* **2000**, *122*, 188–189.
43. Liu, L.; Fan, S. Isotope Labeling of Carbon Nanotubes and Formation of $^{12}C-^{13}C$ Nanotube Junctions. *J. Am. Chem. Soc.* **2001**, *123*, 11502–11503.
44. Boyd, E. J.; Brown, S. A. The Size Dependence of Tin Oxide Atomic Cluster Nanowire Field Effect Transistors. *Nanotechnology* **2009**, *20*, 425201.
45. Sun, J.; Tang, Q.; Lu, A.; Jiang, X.; Wan, Q. Individual SnO_2 Nanowire Transistors Fabricated by the Gold Microwire Mask Method. *Nanotechnology* **2009**, *20*, 255202.
46. Andrei, P.; Fields, L. L.; Zheng, J. P.; Cheng, Y.; Xiong, P. Modeling and Simulation of Single Nanobelt SnO_2 Gas Sensors with FET Structure. *Sens. Actuators, B* **2007**, *128*, 226–234.
47. Hong, W.-K. ; Sohn, J. I.; Hwang, D. -K.; Kwon, S. -S.; Jo, G.; Song, S.; Kim, S. -M.; Ko, H. -J.; Park, S. -J.; Welland, M. E.; et al. Tunable Electronic Transport Characteristics of Surface-Architecture-Controlled ZnO Nanowire Field Effect Transistors. *Nano Lett.* **2008**, *8*, 950–956.
48. Kwon, S.-S.; Hong, W.-K.; Jo, G.; Maeng, J.; Kim, T.-W.; Song, S.; Lee, T. Piezoelectric Effect on the Electronic Transport Characteristics of ZnO Nanowire Field-Effect Transistors on Bent Flexible Substrates. *Adv. Mater.* **2008**, *20*, 4557–4562.
49. Jo, G.; Hong, W.-K.; Sohn, J. I.; Jo, M.; Shin, J.; Welland, M. E.; Hwang, H.; Geckeler, K. E.; Lee, T. Hybrid Complementary Logic Circuits of One-Dimensional Nanomaterials with Adjustment of Operation Voltage. *Adv. Mater.* **2009**, *21*, 2156–2160.
50. Ford, A. C.; Ho, J. C.; Chueh, Y. -L.; Tseng, Y. -C.; Fan, Z.; Guo, J.; Bokor, J.; Javey, A. Diameter-Dependent Electron Mobility of InAs Nanowires. *Nano Lett.* **2009**, *9*, 360–365.
51. Motayed, A.; Vaudin, M.; Davydov, A. V.; Melngailis, J.; He, M.; Mohammad, S. N. Diameter-Dependent Transport Properties of Gallium Nitride Nanowire Field Effect Transistors. *Appl. Phys. Lett.* **2007**, *90*, 043104.
52. Sundaram, V. S.; Mizel, A. Surface Effects on Nanowire Transport: A Numerical Investigation Using the Boltzmann Equation. *J. Phys.: Condens. Matter* **2004**, *16*, 4697–4709.
53. Björk, M. T.; Schmid, H.; Knoch, J.; Riel, H.; Riess, W. Donor Deactivation in Silicon Nanostructures. *Nat. Nanotechnol.* **2009**, *4*, 103–107.
54. Kim, Y. -S.; Lee, K.; Lee, J. S.; Jung, G. Y.; Kim, W. B. Nanoimprint Lithography Patterns with a Vertically Aligned Nanoscale Tubular Carbon Structure. *Nanotechnology* **2008**, *19*, 365305.